A Multi-cancer Detection for Lung and Colon Cancer Using CNN, RNN and Transfer Learning

*

Md. Raihan Tapader
Department of Computer Science & Engineering
DUET, Gazipur, Dhaka, Bangladesh
204006@student.duet.ac.bd

Hasibul Islam
Department of Computer Science & Engineering
DUET, Gazipur, Dhaka, Bangladesh
204056@student.duet.ac.bd

***Abstract*—Lung and colon malignancies are among the most prevalent and deadly cancers worldwide, these cancers account for over 25% of global cancer-related deaths, where early detection is critical for improving patient outcomes. However, current AI-based multi-cancer detection systems face several limitations: (1) poor generalization across different tissue types, (2) inadequate modeling of spatial relationships in histopathological patterns, and (3) limited interpretability, which hinders clinical adoption. In this study, we evaluate four state-of-the-art deep learning models for multi-cancer classification: two CNN-based transfer learning models (ResNet50 and EfficientNet-B0) and two recurrent models (LSTM and BiLSTM). These models achieved impressive classification accuracies of 98.03%, 99.85%, 63.51%, and 94.89%, respectively. Experiments were conducted on the LC25000 dataset, from which 2,676 histopathological image samples with expert annotations were used. This work contributes two main advancements: (1) quantitative evidence of CNN-RNN synergy in histopathology analysis, and (2) establishing benchmark performance on a mid-scale dataset for multi-cancer classification.**

***Index Terms*—Lung cancer, colon cancer, multi-cancer detection, histopathological image analysis, deep learning, CNN, RNN**

I. Introduction

In recent years, deep learning has emerged as a transformative tool in medical image analysis, offering new possibilities for early cancer detection through automated histopathological image classification. Lung and colon cancers, in particular, are major global health concerns due to their high incidence and mortality rates. Accurate diagnosis using histology slides is essential but remains a challenging task due to the complexity and variability of tissue structures. Cancer remains one of the most critical global health challenges, ranking as the second leading cause of death after cardiovascular diseases. In 2018 alone, over 18 million new cancer cases were reported, resulting in approximately 9.5 million deaths worldwide. Among various cancer types, lung and colon cancers are particularly prevalent and lethal, accounting for a significant proportion of global cancer-related mortality in both men and women [1].

Traditional diagnostic methods—such as biopsies and medical imaging—although effective, are often invasive, time-consuming, and costly. Recent advances in artificial intelligence (AI), particularly in deep learning, have opened new frontiers in cancer diagnosis by enabling automated analysis of histopathological images. Convolutional Neural Networks (CNNs) have shown exceptional capability in extracting complex patterns from medical images, leading to improved accuracy in cancer classification.

In this study, we present a hybrid deep learning framework for classifying lung and colon cancers using histopathological images. We evaluate and compare the performance of four models—ResNet50, EfficientNet, LSTM, and BiLSTM—on a subset of the LC25000 dataset. Our approach not only explores the synergy between convolutional and recurrent neural architectures but also investigates how interpretability methods like LIME affect classification performance.

II. Methodology

The proposed methodology follows a structured workflow, as illustrated in Figure 1. After collecting the multi-cancer histopathological dataset, the data is split into three subsets: training (60%), validation (20%), and testing (20%).

These subsets are used to train four different deep learning models: ResNet50, EfficientNet-B0, LSTM, and BiLSTM. Each model is trained independently to learn cancer-specific features from the image data.

Once trained, the models are evaluated using the validation and test sets to assess their performance. The evaluation involves key classification metrics such as accuracy, precision, recall, and F1-score. Finally, the trained models are used for cancer prediction, aiming to support accurate and early diagnosis across multiple cancer types.

A. Datset

The LC25000 [2] dataset consists of 25,000 histopathological images categorized into five classes: lung benign, lung adenocarcinoma, lung squamous cell carcinoma, colon adenocarcinoma, and colon benign tissue. Each class contains 5,000 JPEG images at a resolution of 768×768 pixels. These were generated from 1,250 original samples (750 lung and

Identify applicable funding agency here. If none, delete this.

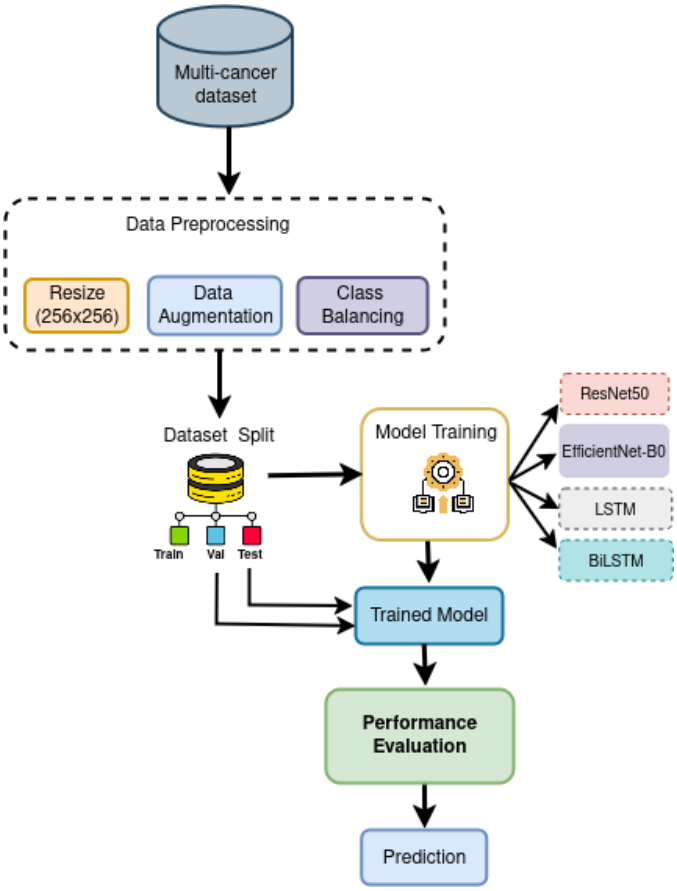

Fig. 1. Proposed approach

500 colon) and expanded through data augmentation using the Augmentor library.

In our study, we used a subset of 2,676 images, which were resized to 256×256 pixels. We further applied augmentation techniques to enhance variability and ensure class balance. The dataset was then split into 60% for training, 20% for validation, and 20% for testing.

III. Results

To assess the performance of our deep learning models, we evaluated four architectures: ResNet50, EfficientNet-B0, LSTM, and BiLSTM. Each model was trained for 10 epochs using an appropriate optimizer and learning rate (LR), and evaluated on a held-out test set. Performance was measured using four key classification metrics: accuracy, precision, recall, and F1-score. Additionally, we used accuracy curves and confusion matrices to visualize model behavior across different tissue classes.

EfficientNet-B0 achieved the highest performance among all models, with an accuracy, precision, recall, and F1-score of 99.85% shown in fig 6 and fig 7. It was trained using the Adam optimizer with a learning rate of 0.001. The confusion matrix confirmed highly accurate predictions across all five tissue classes, with minimal misclassification.

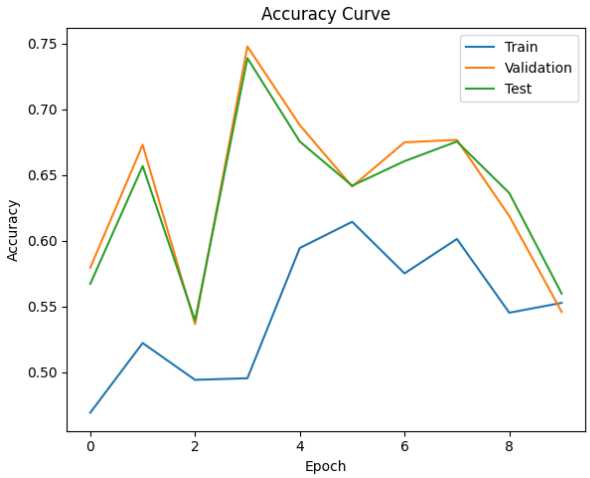

Fig. 2. Training and validation accuracy curves of the LSTM model. The plot illustrates the model's learning progression over epochs, showing convergence behavior and generalization performance across the dataset.

BiLSTM showed strong sequential learning capability with an accuracy of 94.89%, also supported by high precision (94.98%) and recall (94.89%) illustrated in fig 4 and fig 5. It was trained using the AdamW optimizer with a lower learning rate of 0.0005. The confusion matrix and accuracy curve indicated consistent learning and effective temporal pattern recognition.

LSTM, while capturing some temporal features, performed comparatively lower with 63.51% accuracy demonstrated in fig 2 and fig 3. Its confusion matrix revealed considerable misclassifications, particularly between similar tissue types, indicating limitations in handling complex spatial histopathology patterns.

ResNet50 was trained with multiple optimizers (SGD, Adam, and AdamW) during experimentation visualized in fig 8 and fig 9. Although specific accuracy values are not shown here, its performance was noticeably below EfficientNet-B0, suggesting that while effective for image classification, it may require more fine-tuning or deeper architecture for optimal multi-cancer detection.

IV. Conclusion

This research highlights the capability of deep learning approaches in accurately classifying multiple cancer types from histopathological images. Among the models evaluated, EfficientNet-B0 exhibited superior performance, achieving an accuracy of 99.85%, significantly outperforming sequential models such as LSTM and BiLSTM. The implemented methodology comprising image resizing, augmentation, and class balancing contributed to consistent and reliable classification results. These findings underscore the potential of advanced convolutional architectures in enhancing early cancer detection and supporting clinical diagnostic workflows.

TABLE I

THIS TABLE SUMMARIZES THE PERFORMANCE METRICS—ACCURACY, PRECISION, RECALL, AND F1-SCORE—FOR EACH OF THE EVALUATED MODELS, INCLUDING THEIR OPTIMIZER AND LEARNING RATE CONFIGURATIONS.

Model	Optimizer	LR	Accuracy(%)	Precision(%)	Recall (%)	Recall (%)
ResNet50	AdamW	0.001	98.03	98.05	98.05	98.03
EfficientNet-B0	Adam	0.001	**99.85**	**99.85**	**99.85**	**99.85**
LSTM	Adam	0.001	63.51	64.15	63.50	63.16
BiLSTM	AdamW	0.0005	94.89	94.98	94.89	94.87

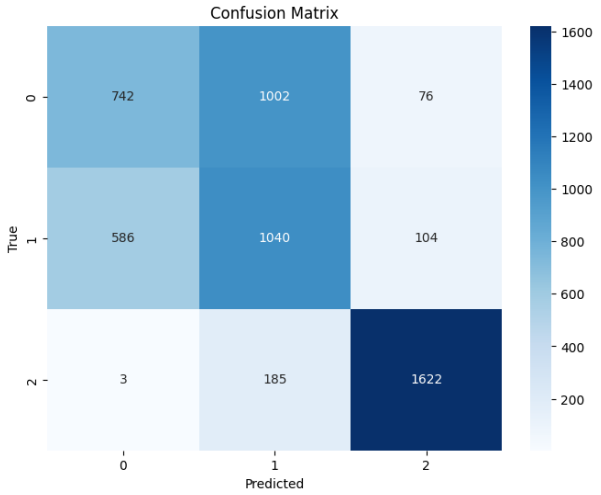

Fig. 3. Normalized confusion matrix for the LSTM model showing classification performance across all five tissue classes. Diagonal elements represent correct predictions, with values indicating percentage accuracy per class.

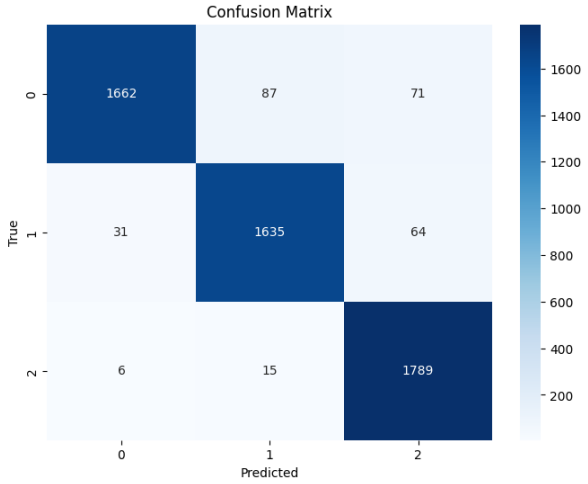

Fig. 5. Normalized confusion matrix for the BiLSTM model showing classification performance across all five tissue classes. Diagonal elements represent correct predictions, with values indicating percentage accuracy per class.

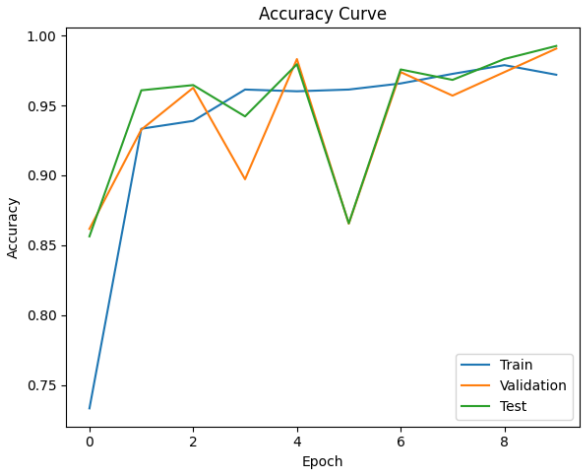

Fig. 4. Training and validation accuracy curves of the BiLSTM model. The plot illustrates the model's learning progression over epochs, showing convergence behavior and generalization performance across the dataset.

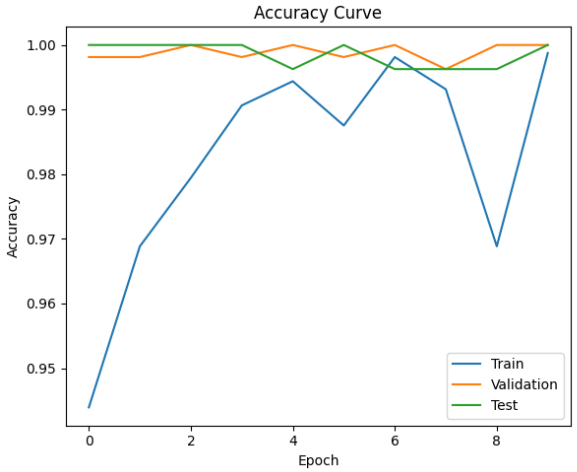

Fig. 6. Training and validation accuracy curves of the EfficientNet-B0 model. The plot illustrates the model's learning progression over epochs, showing convergence behavior and generalization performance across the dataset.

REFERENCES

[1] M. R. Karim, A. Rahman, and R. Islam, "A multi-cancer detection and localization system utilizing x-ai and ensemble technique using cnn," in *2024 6th International Conference on Electrical Engineering and Information & Communication Technology (ICEEICT)*. IEEE, 2024, pp. 475–480.

[2] A. A. Borkowski, M. M. Bui, L. B. Thomas, C. P. Wilson, L. A. DeLand, and S. M. Mastorides, "Lung and colon cancer histopathological image dataset (lc25000)," *arXiv preprint arXiv:1912.12142*, 2019.

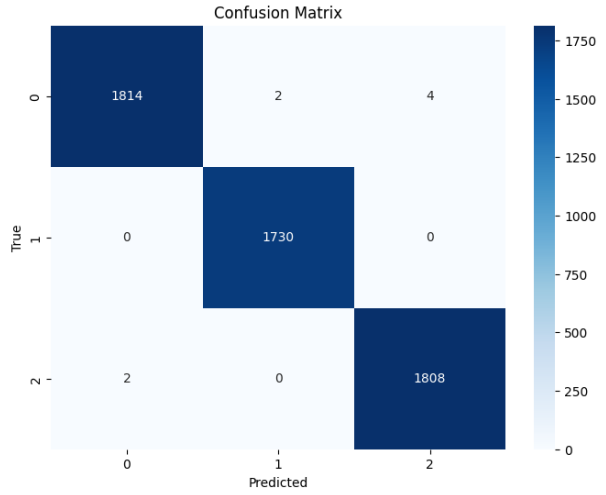

Fig. 7. Normalized confusion matrix for the EfficientNet-B0 model showing classification performance across all five tissue classes. Diagonal elements represent correct predictions, with values indicating percentage accuracy per class.

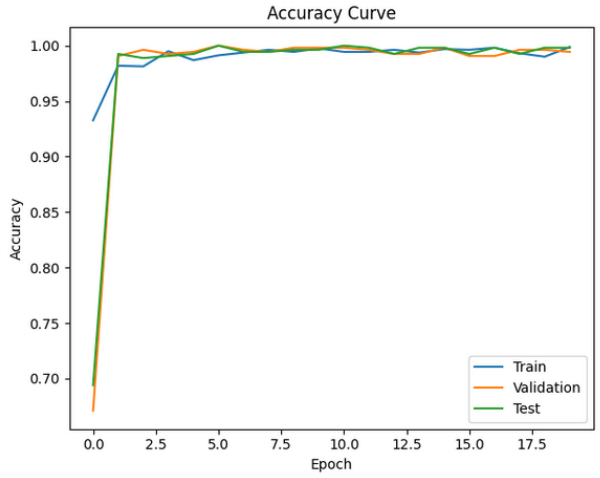

Fig. 8. Training and validation accuracy curves of the ResNet50 model. The plot illustrates the model's learning progression over epochs, showing convergence behavior and generalization performance across the dataset.

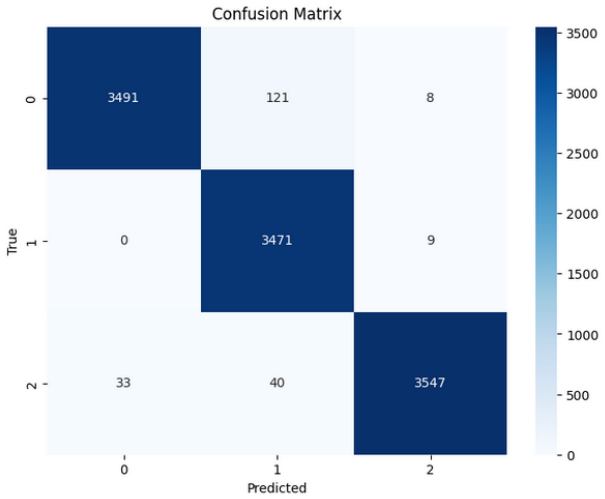

Fig. 9. Normalized confusion matrix for the ResNet50 model showing classification performance across all five tissue classes. Diagonal elements represent correct predictions, with values indicating percentage accuracy per class.